

## Tribological properties of Al/diamond composites produced by cold spray additive manufacturing

Chaoyue Chen<sup>a</sup>, Yingchun Xie<sup>b,\*</sup>, Xingchen Yan<sup>b,\*</sup>, Mansur Ahmed<sup>c</sup>, Rocco Lupoi<sup>c</sup>, Jiang Wang<sup>a</sup>, Zhongming Ren<sup>a</sup>, Hanlin Liao<sup>d</sup>, Shuo Yin<sup>c,\*</sup>

<sup>a</sup> State Key Laboratory of Advanced Special Steels, School of Materials Science and Engineering, Shanghai University, Shanghai 200444, PR China

<sup>b</sup> National Engineering Laboratory for Modern Materials Surface Engineering Technology, The Key Lab of Guangdong for Modern Surface Engineering Technology, Guangdong Institute of New Materials, Guangzhou 510651, PR China

<sup>c</sup> Trinity College Dublin, The University of Dublin, Department of Mechanical and Manufacturing Engineering, Parsons Building, Dublin 2, Ireland

<sup>d</sup> ICB UMR 6303, CNRS, Univ. Bourgogne Franche-Comté, UTBM, F-90010 Belfort, France



### ARTICLE INFO

**Keywords:**

Cold spray  
Diamond  
Aluminum matrix composite  
Grain refinement  
Wear performance

### ABSTRACT

A range of Al/diamond metal matrix composites using advanced core-shell structured diamond powders was fabricated employing solid-state cold spray additive manufacturing technology. Cold spray technique combined with core-shell structured diamond particles has demonstrated excellent capability to produce dense Al/diamond composites with superior tribological properties. The core-shell structured diamond was easier to deposit than pure Al by cold spray, particularly under low particle impact velocity, implying high potentials as preferential feedstock for cold spray. The wear-resistance performance of the Al/diamond composites produced by nitrogen and helium were investigated. Wear test illustrated that the Al/diamond composites had superior wear-resistance properties comparable to the selective laser melting Inconel 625 and 17–4PH alloys. Higher diamond contents in the composites resulted in better wear resistance. Based on the worn track analysis via X-ray computed tomography, the role of the diamond reinforcement in improving the wear-resistance performance was also clarified.

### 1. Introduction

Al and its alloys have been widely used in the sectors of aerospace, automotive, and construction due to their low density and excellent corrosion-resistance property. Due to the well-known poor wear-resistance performance, the Al components always suffer from severe wear and erosion during routine service, which significantly reduces their service time and limits their application. In contrast, diamond is known to possess extremely high hardness, which allows it to be used as an excellent wear-resistance material. However, unlike metals, diamond is generally small in size and difficult to be shaped and machined. This fact, in turn, limits the direct application of pure bulk diamond in the modern industry.

Diamond-reinforced Al matrix composite (Al/diamond) is a novel material, which can gain the benefits of both Al and diamond. Al acts as a binder phase yielding machinability, while diamond reinforcements improve the wear-resistance performance of the Al matrix. Currently, Al/diamond composites were mainly produced through metal infiltration [1–3] (i.e., gas pressure infiltration, liquid metal infiltration, and

pressureless infiltration) and powder metallurgy (spark plasma sintering and hot pressing) [4–10]. As high-temperature processes, metal infiltration is known to lead to inhomogeneous dispersion of diamond reinforcements in the composite, graphitization of the diamond, and formation of brittle Al<sub>4</sub>C<sub>3</sub> phase at the interface of diamond and molten Al, which may be harmful to the composite properties [9,11–14]. Powder metallurgy can produce Al/diamond composite at the lower sintering temperature, preventing the occurrence of phase transformation at the interfaces, but low processing temperature tends to result in weak interfacial bonding and thus reduce the composite performance [7,15]. Moreover, both technologies are only applicable for producing simple-geometry raw materials but unsuitable for near-net-shape complex structures [16]. Spark plasma sintering, in particular, needs much higher processing cost than other methods. These drawbacks are promoting the development of a low-cost and low-temperature technology for the fabrication of high-quality Al/diamond composite with complex structures. Selective laser melting (SLM), a powder-bed additive manufacturing technology [17,18] was reported to fabricate the diamond reinforced Al alloy composites [19]. However, due to the high

\* Corresponding authors.

E-mail addresses: [yingchun.xie@hotmail.com](mailto:yingchun.xie@hotmail.com) (Y. Xie), [yanxingchen@gdinm.com](mailto:yanxingchen@gdinm.com) (X. Yan), [yins@tcd.ie](mailto:yins@tcd.ie) (S. Yin).

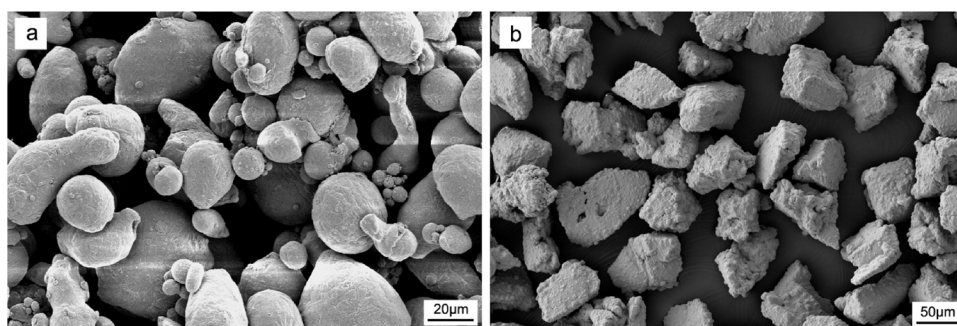


**Fig. 1.** Morphology of the feedstock powders used in this study: (a) Al and (b) Cu-Ni-coated diamond.

thermal conductivity of the diamond particle and high cooling rate of the molten pool, the high porosity and the formation of the  $\text{Al}_4\text{C}_3$  brittle phase in the SLM composites cannot be avoided.

Cold spray is an emerging additive manufacturing and coating technology. In this process, micro-scale powders are accelerated by a supersonic gas passing through a de-Laval nozzle and subsequently impact onto a substrate to form a coating or bulk deposit [20,21]. Metals [22,23], metal matrix composites [24,25], and even ceramics [26] have been successfully deposited onto various substrates via cold spray without exceeding their melting points. Defects encountered in the related high-temperature deposition processes such as oxidation, thermal residual stress, and phase transformation can be effectively avoided [27–30]. Cold spray can fabricate materials with complex structures, produce thin-film coatings, and also repair damaged components [31,32]. As compared with laser-based additive manufacturing technologies, the cold spray also has many unique advantages such as high efficiency, low cost, and low porosity. Particularly, for Al-based materials with high reflectivity and thermal conductivity, cold spray additive manufacturing demonstrates an incomparable advantage [17,33,34].

To date, a large number of studies have been done to investigate cold sprayed Al-based composites for wear-resistance. It is reported that dense Al-based wear-resistant composites can be produced by cold spray, reducing the wear rate by order of magnitude as compared with pure Al [35–37]. However, state-of-the-art also suggests that there still exist limitations for fabricating Al-based composites via cold spray. On the one hand, the commonly used reinforcement particles for Al matrix (i.e.,  $\text{Al}_2\text{O}_3$  [38],  $\text{SiC}$  [36,37],  $\text{TiN}$  [39,40],  $\text{BN}$  [41,42] and  $\text{B}_4\text{C}$  [43]) are not sufficiently hard, which significantly limits the wear-resistance performance of the composites. On the other hand, the existing preparation methods of powder feedstock (i.e., mechanical mixing and ball milling) are not efficient. The mechanically pre-mixed powders frequently lead to a reduction in the reinforcement content in the deposits compared to in the original feedstock [37,42]. The ball-milling procedure always results in the degradation of feedstock particles, which is harmful to the coating cohesion strength [44,45]. By taking all the aforementioned issues into account, the composite powders with a core-shell structure have been proposed to produce high-quality composite deposits using a cold spray technique [24,25,46]. Such composite powder is composed of a ductile metal shell and a hard or brittle core. The metallic shell can experience server plastic deformation during high-velocity impact, resulting in a metallurgical bonding with the

substrate or previously deposited materials and promoting the co-deposition of the composites.

Therefore, in this paper, the novel cold spray additive manufacturing process was applied with the core-shell-structured powders to fabricate light and machinable Al/diamond composites with excellent wear-resistance performance. Cu-Ni-coated diamond particles were used as the feedstock to improve the diamond deposition efficiency and to increase diamond content in the composites introducing a practical metal-to-metal bond between the Al matrix and diamond reinforcement [24]. Following the fabrication of the Al/diamond composites at different working parameters, their composition, phase transformation, microstructure, and tribological properties were studied in detail. The Al/diamond composites produced in this work can be used as additive manufactured materials, functional coatings, or as back-filling materials for repairing damaged components.

## 2. Experimental methodology

### 2.1. Composite fabrication

Commercially available pure spherical Al powder (Valimet, USA) with a size distribution ranging between 15 and 58  $\mu\text{m}$  ( $D_{25} = 22 \mu\text{m}$ ,  $D_{50} = 32 \mu\text{m}$ , and  $D_{75} = 48 \mu\text{m}$ ) and irregular Cu-Ni-coated diamond powders (PDA C50, Element-Six, Ireland) with a size range of 45–53  $\mu\text{m}$  were applied as the feedstock materials for cold spray in this work. Fig. 1 shows the morphology of the feedstock powders observed using scanning electron microscopy (SEM, Carl Zeiss ULTRA, Germany). The Cu-Ni-coated diamond particle consists of a diamond core, an electroless Ni nanolayer, and an electroless thin Cu layer with only a few microns. According to the supplier, the weight ratio of the diamond phase to both metals in a single particle is approximately 1:1. The detailed inner structure of the Cu-Ni-coated diamond particle can be found elsewhere [24,46].

The Al/diamond composites were deposited onto pure Al substrates using an in-house cold spray system based in Trinity College Dublin, Ireland. The system consists of high-pressure nitrogen/helium gas from cylinders, gas heater, powder feeder, CNC working platform for controlling the substrate movement, de-Laval nozzle, and computer control system. The spraying nozzle made of WC-Co has a throat diameter and an exit diameter of 2 mm and 6 mm, respectively, with a total length of 210 mm. The Al and Cu-Ni-coated diamond powders were mechanically mixed in different ratios before spraying. The detailed feedstock

**Table 1**

Annotation of the produced coatings, the respective feedstock composition, and cold spray deposition conditions.

Annotation	Powder	Diamond volume content [%]	Gas type	Pressure [MPa]	Temperature [ $^{\circ}\text{C}$ ]
N <sub>4-1</sub>	Al + Cu-Ni-coated diamond (4:1 by weight)	8.5	Nitrogen	3.0	400
N <sub>1-1</sub>	Al + Cu-Ni-coated diamond (1:1 by weight)	25.1	Nitrogen	3.0	400
H <sub>4-1</sub>	Al + Cu-Ni-coated diamond (4:1 by weight)	8.5	Helium	3.0	25
H <sub>1-1</sub>	Al + Cu-Ni-coated diamond (1:1 by weight)	25.1	Helium	3.0	25

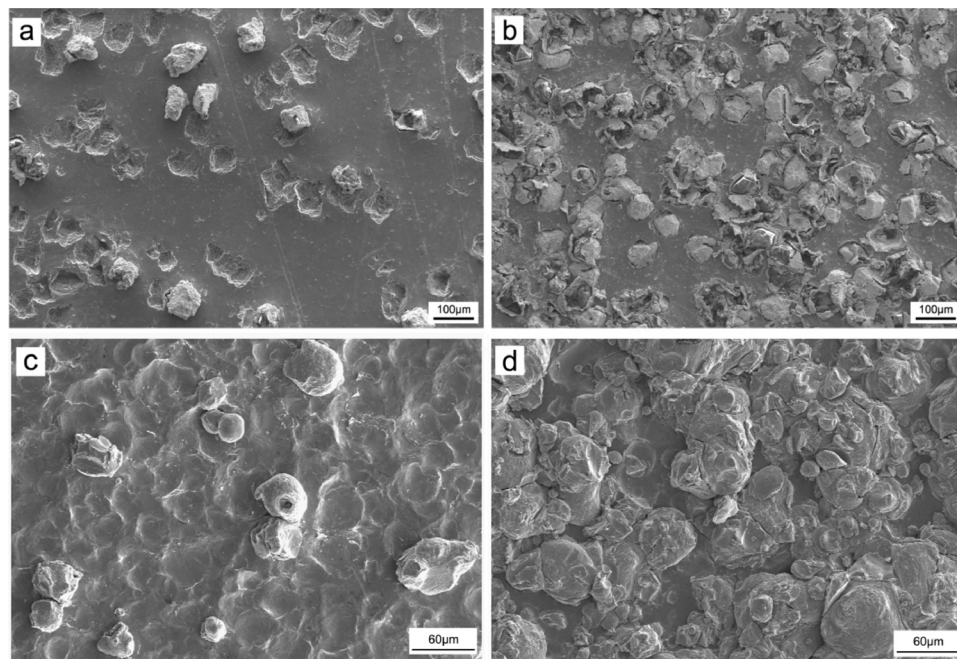


**Fig. 2.** Surface morphology of the cold sprayed Al substrate after impacted by Cu-Ni-coated diamond and Al particles using nitrogen and helium propulsive gases: (a) Cu-Ni-coated diamond particles deposited by nitrogen, (b) Cu-Ni-coated diamond particles deposited by helium, (c) Al particles deposited by nitrogen and (d) Al particles deposited by helium.

information and cold spray deposition conditions are provided in [Table 1](#). The gas pressure was measured using a pressure gauge installed on the pipeline transporting propulsive gas, and the gas temperature was measured by a thermocouple placed in front of the nozzle inlet. The powders were injected into the nozzle at the nozzle inlet without preheating. To prevent the clogging of the nozzle, a self-made cooling jacket was applied and installed on the nozzle exterior wall. Both nitrogen and helium were used as the propulsive gas to produce the composites in this work. For facilitating the following discussion, each composite was given an annotation. The annotation 'N' means nitrogen-produced composites, while 'H' indicates helium-produced composites. In order to obtain a roughly same composite thickness, the nitrogen-produced and helium-produced composites were fabricated with 12 and 2 gun passes, respectively. All deposits were produced at a stand-off distance of 35 mm and a traversal speed of 50 mm/s. The wheel rotating speed of the powder feeder was set as 30 %.

The deposition of single Al and Cu-Ni-coated diamond particles were also carried out in this work. Cold sprayed pure Al was used as the substrate. The cold sprayed Al substrate was produced using the working conditions given in [Table 1](#). The as-fabricated Al was then polished using standard metallographic procedures with the final polishing applied by 0.05 μm SiC solution. The Al and Cu-Ni-coated diamond were deposited onto the polished Al substrate at a fast traversal speed of 200 mm/s to produce the single deposited particles.

## 2.2. Material characterization

In order to investigate the phase transformation of the composites during cold spray, the composites were examined using an X-ray diffractometer (XRD, Siemens D500, Germany) with the Co ( $\lambda = 1.789 \text{ \AA}$ ) source at a current of 40 mA, a voltage of 35 kV and scan step of 0.02°. To assess the composite microstructure and element analysis, all samples were prepared using standard metallographic procedures with the final polishing applied by 1 μm diamond solution. The EDS element mapping of a single deposited Cu-Ni-coated diamond particle in the composite was also conducted on the polished cross-section.

The diamond volume content in the composites was calculated based on binary image analysis. The binary image analysis was performed on the cross-sectional micrographs using the Image J software. For each sample, five images were used to calculate the average value.

To further understand the diamond particle distribution and content in the composite, the composite samples were also examined using an X-ray computer tomography (XCT) (X5000, North Star Imaging, USA). A cylinder sample with a dimension of  $\Phi 3 \times 5 \text{ mm}^3$  was scanned to obtain the diamond content under different processing conditions. The samples were placed on the rotating stage in front of the X-ray source with a precision of 4 μm/voxel. The tomography was operated at an acceleration voltage of 100 keV and a current of 90 μA. The 3D reconstruction was realized using the Amira-Avizo software (FEI Visualization Sciences Group, Software, Germany). The bonding ratio of Al and Cu-Ni-coated diamond particles onto the cold sprayed pure Al substrates were measured. The bonding ratio was determined as  $BR = N_D/N_T$ , where  $N_D$  is the number of deposited particles, and  $N_T$  is the total impacting particles (sum of the number of deposited particles and craters).

## 2.3. Tribological property test

The microhardness of the composites was tested by a Vickers hardness indenter (Mitutoyo, Japan) with a load of 9.8 N for 10 s. The indentation was taken at the Al matrix area to avoid the influence of the diamond particles. A total of 15 values were averaged to determine the microhardness. The tribological properties were measured using a ball-on-disc tribometer (UMT-3, Bruker, USA) at room temperature. For accurate measurement of the wear rates, the sample surfaces were polished using the diamond solution to 6 μm roughness prior to the test, and the samples were then mounted on a carrier disc. A tungsten carbide ball with a diameter of 10 mm was used as a counterpart under a constant load of 20 N. The disk rotated at a linear speed of 50 mm/s for a sliding distance of 360 m. To determine the coating wear rates, the material volume loss was calculated according to ASTM G 99 standard [47]. The wear rate was then calculated as the volume loss per unit load and per traverse distance. The worn samples after tribological tests were studied using SEM, EDS, and also XCT.

## 3. Results and discussion

### 3.1. Individual particle deposition behavior

[Fig. 2](#) shows the surface morphology of the cold sprayed Al substrate

after impacted by Cu-Ni-coated diamond and Al particles using different propulsive gases. The bonding ratios of the Al and Cu-Ni-coated diamond particles driven by nitrogen were  $7.3 \pm 2.5\%$  and  $27.5 \pm 3.6\%$  respectively, and for helium, the values were  $> 95\%$  and  $97.5 \pm 2.1\%$  respectively. Note that the bonding ratio of helium-driven Al particles is an estimated value due to the difficulty in determining the number of impact particles. From Fig. 2, two apparent differences can be identified. Firstly, for both Cu-Ni-coated diamond and Al particles, the use of helium as the propulsive gas resulted in a much higher bonding ratio than using nitrogen. The bonding ratio of helium-driven Cu-Ni-coated diamond reached nearly 100%, approximately four times higher than that of nitrogen-driven one. The same situation was also seen in Al particles, where the discrepancy was more than ten times. This is due to the better particle ‘pick-up’ capability of low-molecular helium than nitrogen and the resultant higher particle impact velocity [48].

The deposition mechanism of the core-shell composite particle in the cold spray process has attracted great research interest [46]. The single splat deposition can directly reveal the deformation behavior of the shell and interior core parts. Thus, to investigate the deformation behavior of the Cu-Ni-coated diamond particles, a single splat experiment was conducted. Fig. 3 shows the surface morphology of the single Cu-Ni-coated diamond particles deposited on the Al substrate using different propulsive gases. It is known that the higher impact velocity of the composite particle can be obtained when using helium as the propulsive gas. As can be seen, the nitrogen-driven Cu-Ni-coated diamond particles shallowly adhered to the surface substrate without significant penetration due to the low impact energy, as shown in Fig. 3a, and b. In contrast, as the helium-driven particles gained higher impact velocity and kinetic energy, they deeply penetrated into the substrate, causing large-scale plastic deformation of the Al substrate, as shown in Figs. 3c and 4 d. Such large-scale plastic deformation of the soft substrate can induce strong mechanical interlocking between particles and substrate, and lead to higher bond strength [49,50]. In addition, the ductile metal shell of the Cu-Ni-coated diamond particles driven by helium can experience more severe plastic deformation, which may promote its metallurgical bonding with the Al substrate and hence further improve the bond strength [46].

These phenomena may partially explain the reason why the bonding

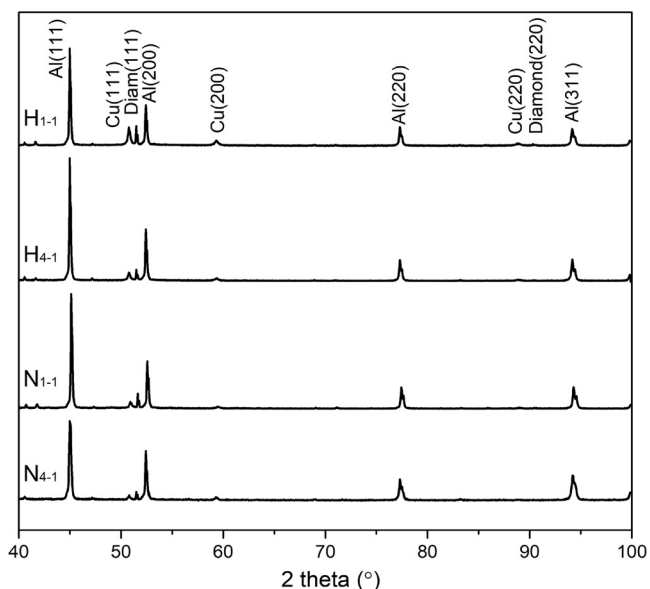


**Fig. 4.** XRD spectra of the Al/diamond composites produced under different conditions.

ratio of helium-driven Cu-Ni-coated diamond particles had a higher bonding ratio. In addition, from Fig. 3, the fracture can also be seen for some Cu-Ni-coated diamond particles after deposition. Due to the difference in particle impact energy, low-velocity impact only resulted in cracks of the outside Cu-Ni layer without fracture of the diamond core, as shown in Fig. 3b, which was also reported on the composite particle with a core-shell structure elsewhere [25]. However, the high-velocity impact caused delamination of the metal layer and even cracking of the diamond core, as shown in Fig. 3d.

### 3.2. Composition and microstructure

Fig. 4 shows the XRD spectra of the Al/diamond composites produced under different conditions. The detected peaks reveal that all

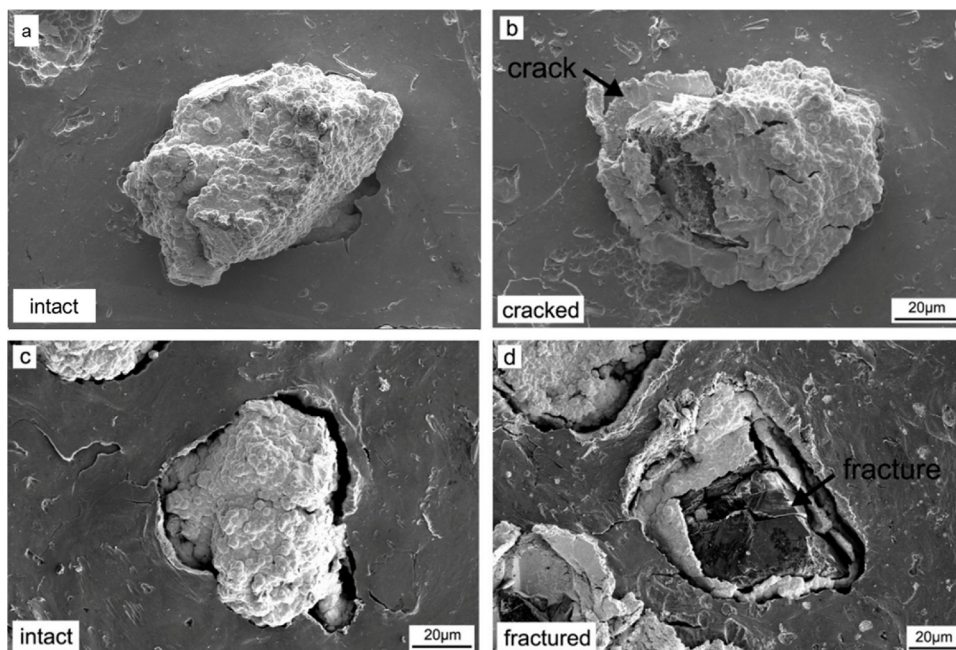


**Fig. 3.** Surface morphology of the Cu-Ni-coated diamond particles deposited on the cold sprayed Al substrate: (a, b) deposited by nitrogen and (c, d) deposited by helium.

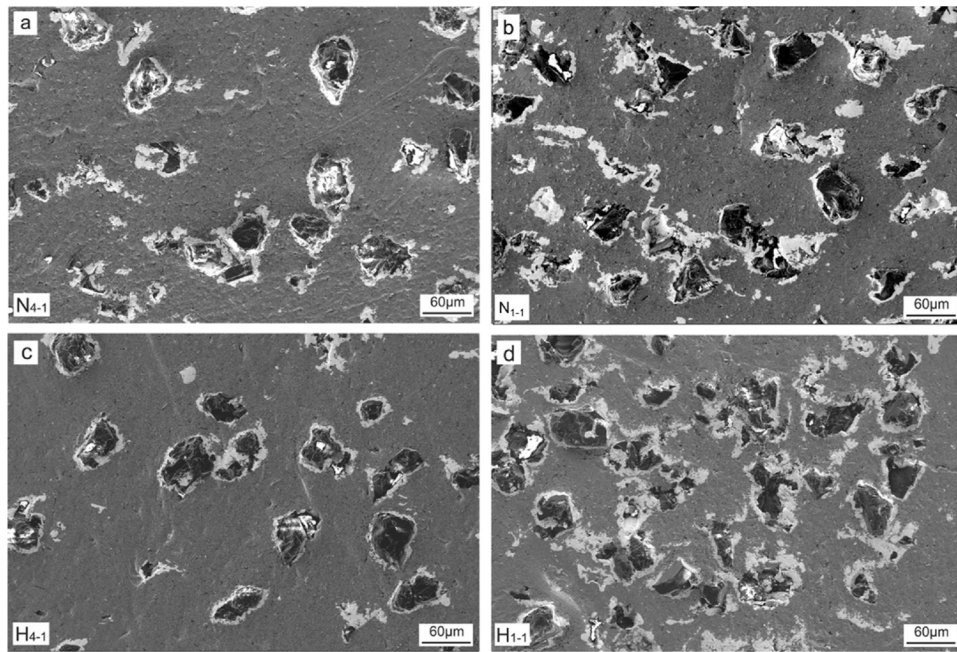
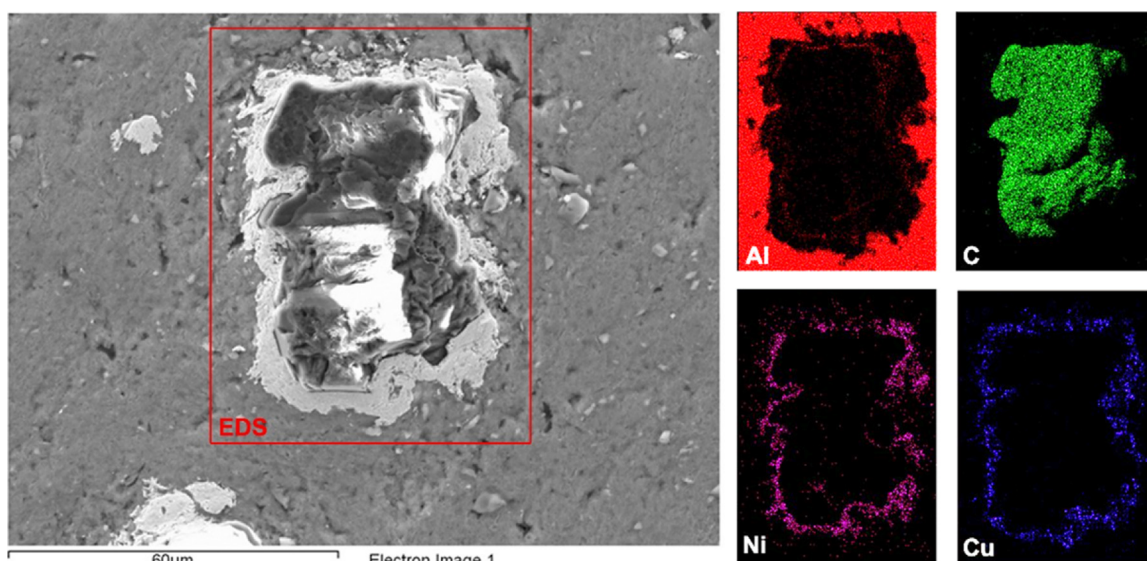


**Fig. 5.** SEM imaging of the cross-section of the Al/diamond composites produced under different conditions.

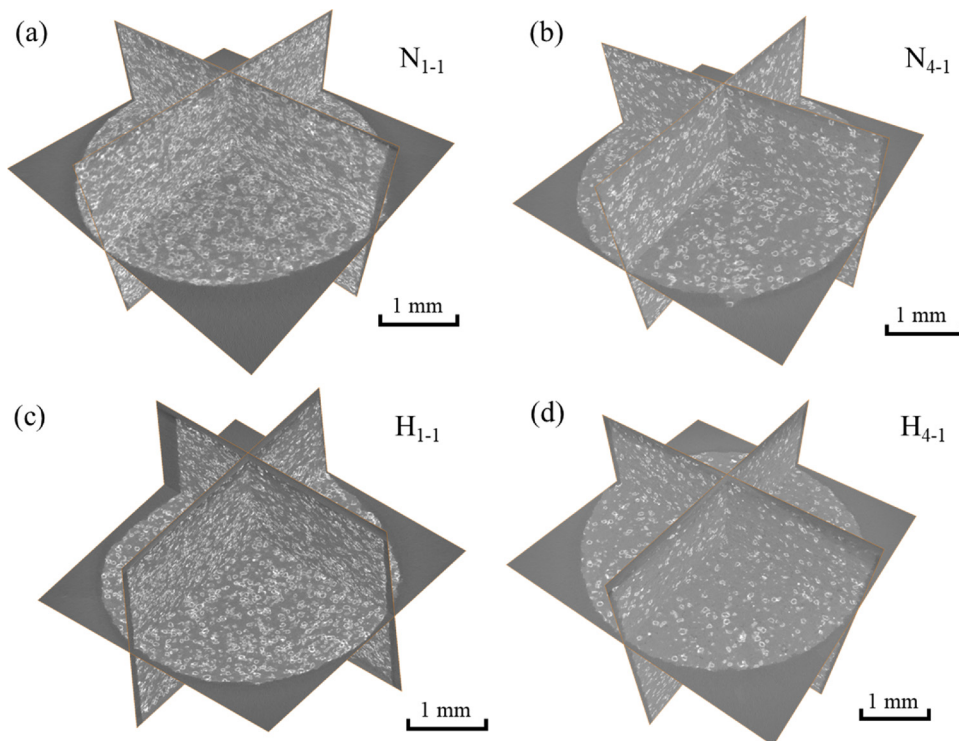
composites containing Al, Cu, Ni, and a diamond without graphitization occurred during the cold spray process, which demonstrates the advantage of cold spray over the other high-temperature techniques in preventing diamond graphitization [24,51].

Fig. 5 shows the cross-section image of the Al/diamond composites produced under different conditions. For all samples, the uniform distribution of the diamond reinforcements can be clearly observed from the cross-section image. This is very important to the composite performance as a uniformly distributed hard phase is beneficial to the overall properties [52–54]. In addition, it is also seen that most of the diamonds in the composites had a diameter of approximately 40–50 μm, which is comparable to the diamond core diameter in the original feedstock (-47 + 40 μm). This fact indicates that most diamond particles did not exhibit substantial fracturing during deposition due to the ‘buffering effect’ of the soft matrix phase [51]. To better investigate the deposition behavior of Cu-Ni-coated diamond within the composite, EDS mapping of a Cu-Ni-coated diamond particle within the N<sub>4-1</sub>

composite is investigated (Fig. 6). It is seen that the Cu-Ni-coated diamond particle completely retained its original core-shell structure in the composite. The diamond core was surrounded by the metal layers, which intimately contacted with the Al matrix. Such direct metal-to-metal contact provided the essential condition for the possible metallurgical inter-particle bonding mechanism [46]. Moreover, despite the fact that most of the diamond particles were intact after deposition, there were still a small number of fractured diamonds or diamond fragments in the composites, as can be identified in Fig. 5. Such fracture was induced by either the high-velocity impact, as shown in Fig. 3d or the inter-particle impact between two Cu-Ni-coated diamond, which is inevitable during cold spray [24,25]. For further characterizing the diamond particles in the composites, Fig. 8 provides the XCT reconstruction results of three characteristic slices taken from vertical, horizontal and transversal plane of the composite samples. It is seen that the diamond particles were uniformly distributed in all composites, which is in good consistency with the SEM observation.



**Fig. 6.** Microstructure and EDS mapping of an intact Cu-Ni-coated diamond in the N<sub>4-1</sub> composite.



**Fig. 7.** Slice from the vertical, horizontal, and transverse planes taken within the XCT reconstruction results, showing the diamond particle on each slice.

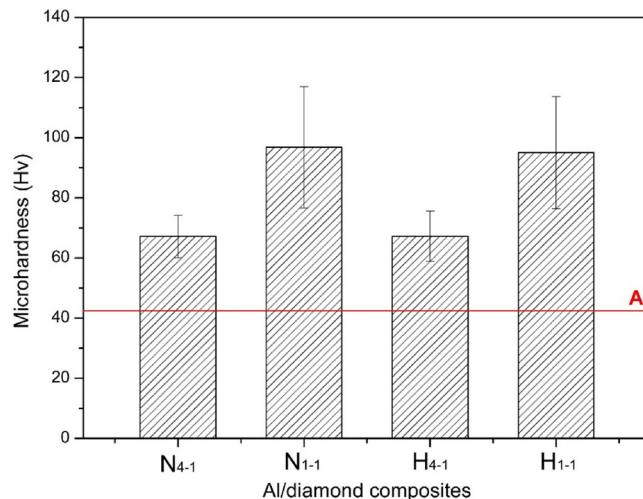


**Fig. 8.** Microhardness of the Al/diamond composites, and the microhardness of cold sprayed pure Al was also provided and highlighted with a red line.

In addition, it is noticed in Fig. 7 that the diamond contents in different composites are different. For the quantitative study, the

volume content and retainability of the diamond in the Al/diamond composite samples were examined through OM image analysis and XCT reconstruction, and the results are provided in Table 2. It can be found that the propulsive gas of helium with a better particle acceleration behavior cannot prominently improve the diamond content in the composite sample. This phenomenon can be well explained by the particle bonding ratio, as discussed in Section 3.1. Both Al and Cu-Ni-coated diamond particles had a similar bonding ratio (> 95 %) under the helium condition. However, under nitrogen condition, Cu-Ni-coated diamond particles had a higher bonding ratio than that of Al, which means more Cu-Ni-coated diamond particles can be successfully deposited than Al. In terms of the diamond retainability, all composites showed superior diamond retainability as compared with conventional cold sprayed MMCs (i.e., using un-coated ceramic or diamond powders) [35,55,56], clearly indicating the significance and benefits of the core-shell structured powders for cold spray.

### 3.3. Tribological property

Fig. 8 shows the microhardness of the Al/diamond composites produced in this work. It is clear that the hardness of all Al/diamond composites was higher than the cold sprayed pure Al deposit due to the dispersion strengthening effect of diamond reinforcements. In addition, higher diamond content in the composites resulted in higher

**Table 2**

Diamond volume content in the Al/diamond composites and its retainability obtained by OM and CT observation. Note that diamond retainability is defined as the ratio of diamond in the composite to in the original feedstock.

Sample ID	In feedstock	OM		XCT	
		Volume content in the composite	Retainability	Volume content in the composite	Diamond retainability
N <sub>4-1</sub>	[%]	7.13 ± 1.48	83.88 ± 17.39	7.76	91.29
N <sub>1-1</sub>	8.5	17.35 ± 1.32	69.12 ± 5.26	20.65	82.27
H <sub>4-1</sub>	25.1	6.48 ± 1.43	76.72 ± 16.85	7.06	83.06
H <sub>1-1</sub>	8.5	16.42 ± 2.31	65.40 ± 9.18	19.13	76.22

**Table 3**

Wear rates ( $\text{mm}^3/\text{N}\cdot\text{m}$ ) of the Al/diamond composites after the ball-on-disk test.

Sample	$\text{N}_{4-1}$	$\text{N}_{1-1}$	$\text{H}_{4-1}$	$\text{H}_{1-1}$	SLM 17–4 PH	SLM Inconel 625
Wear rate	$1.08 \times 10^{-4}$	$3.55 \times 10^{-5}$	$1.23 \times 10^{-4}$	$3.25 \times 10^{-5}$	$1.95 \times 10^{-5}$	$5.37 \times 10^{-5}$

microhardness due to the enhanced dispersion strengthening effects [42,44,57]. However, propulsive gas type, in other words, particle impact velocity, had no effect on the microhardness (see Fig. 8). Such similarity in hardness regardless of the propulsive gas type can be discussed using the diamond content given in Table 2. The similar hardness value indicates that the work-hardening effect was nearly the same in the nitrogen- and helium-produced composite samples. For the helium-produced sample, the work-hardening effect was mainly caused by the severe plastic deformation of the Al particles during their deposition. However, for the nitrogen-produced sample, despite the lower particle velocity, the lower bonding ratio can lead to a more significant in-process peening effect due to the rebounding particles. Such an in-process peening effect also induced extensive working-hardening effect and thus resulted in a comparable microhardness [58,59]. This fact may imply that the microhardness of cold sprayed composites is not determined by the deformation-induced work hardening of the soft matrix phase but by the dispersion strengthening of reinforcements.

Table 3 shows the wear rates of the Al/diamond composites after the ball-on-disk test. It is seen that the  $\text{N}_{1-1}$  and  $\text{H}_{1-1}$  composites exhibited better wear resistance performance than the  $\text{N}_{4-1}$  and  $\text{H}_{4-1}$ , respectively, due to much higher diamond contents. Similarly, because of the close diamond contents between the nitrogen-produced and helium-produced composites, an equivalent wear resistance performance was achieved for them. From the perspective of overall manufacturing cost, nitrogen is much more economical than helium, but using nitrogen as propulsive gas may lead to much more diamond powder waste than using helium due to the lower diamond deposition efficiency. Therefore, it is not easy to make a judgment in this work in which manufacturing strategy is more economical. Furthermore, the fully dense samples of 17–4PH stainless steel and Inconel 625 alloy with high hardness value and anti-wear performance were fabricated by SLM using optimal operation parameters. The wear rate values are compared with the cold sprayed Al/diamond composites in order to demonstrate the superiority, where the comparison is given in Table 3. It should be noted that the microhardness of the SLM 17–4PH and Inconel 625 alloys under as-built conditions are  $334 \text{ Hv}_{0.3}$  and  $236 \text{ Hv}_{0.3}$ , respectively. It is clearly seen that the  $\text{N}_{1-1}$ ,  $\text{H}_{4-1}$ , and  $\text{H}_{1-1}$  Al/diamond composites exhibited superior wear-resistance property, which is comparable with the SLM 17–4PH steel and Inconel 625 alloy with notably higher hardness value.

To further investigate the wear mechanism, the worn surfaces of the Al/diamond composites are examined as shown in Fig. 9. Exposed diamond particles of all Al/diamond composites can be found on the worn surface. It is evident that the diamonds were not removed or peeled off from but rather remained embedded in the composites, which prevented the counterpart from wearing the Al phase of the composites. From the insert images in Fig. 9, the  $\text{H}_{1-1}$  sample exhibited a narrower worn track than the  $\text{H}_{4-1}$  sample indicating a lower worn volume and a shallow indentation of the counterpart into the composite surface during the tribological test. To further identify the composites' tribofilm, EDS mapping of the worn surface of the  $\text{H}_{1-1}$  sample is provided in Fig. 10. Evidently, the worn surface was covered by disconnecting tribofilm composed of W and O. Such an element mixture indicates that the counterpart was severely worn during sliding. The WC debris worn off from the counterpart was crushed during the continuous sliding process, forming thick tungsten carbide film on the worn surface, which then acted as a protecting layer to further prevent the wear of the underneath composites. Additionally, by comparing the four worn surfaces, it is found that the thickness of the WC film

exhibited a significant difference. The  $\text{H}_{4-1}$  and  $\text{N}_{4-1}$  samples showed a relatively connecting tribofilm with some cracks on the surface. This is due to the lower contact stress during sliding as a result of lower diamond content and hardness, higher contact area in the  $\text{H}_{4-1}$  and  $\text{N}_{4-1}$  samples. However, the WC films on the worn surfaces of  $\text{H}_{1-1}$  and  $\text{N}_{1-1}$  samples are rather disconnecting because of the higher diamond content.

Then, the XCT examination was performed on the worn samples to further reveal the wear mechanism and the diamond distribution on the worn track. It should be noted that the worn track radius is equal in spite of the different scale bars. As shown in Fig. 11(a) and (c), the XCT reconstruction of the worn track of the  $\text{H}_{1-1}$  and  $\text{H}_{4-1}$  composites were illustrated, with gray and blue parts indicating Al and diamond phase, respectively. Fig. 11(b) and (d) show the diamond phase within the worn samples obtained from the composite by subtracting the Al phase. By comparing the worn track and the scale bar, the  $\text{H}_{1-1}$  sample evidently displays a smaller worn area than that of  $\text{H}_{4-1}$ , which is in good consistency with the SEM observation (see Fig. 5). Besides, as can be seen from Fig. 11(a), few diamond particles were exposed on the worn track, which agrees well with the element mapping via EDS (see Fig. 10). On the contrary, the worn track was mostly covered by the tribofilm composed by Al, tungsten carbide, and their oxide, which was formed due to continuous sliding and friction during the tribological test. As can be seen from Fig. 11(b), a continuous diamond track existed beneath the surface tribofilm, which represents a distinct morphology compared to the as-sprayed composite coating. During the tribological test, the diamond particles on the coating surface area experienced cyclic loading and compacting by the counterpart. The aggregations of diamond particles were found underneath the tribofilm on the worn track. The reinforcing diamond particles significantly improve the wear resistance against the friction of the counterpart. As the  $\text{H}_{4-1}$  sample is shown in Fig. 11(c) and (d), more diamond particles were exposed on the worn track, which indicates a more serious abrasion of Al during the successive sliding.

#### 4. Conclusions

In this paper, a range of Al/diamond composites was fabricated employing the solid-state cold spray additive manufacturing using advanced core-shell structured diamond powders. The cold spray combined with core-shell structured diamond particles has demonstrated super capability to produce Al/diamond composites with excellent tribological properties. Based on the experimental results and thorough discussion, the following important conclusions were drawn:

- 1 The core-shell structured diamond was deposited more easily than pure Al, showing great potentials as feedstock for cold spray.
- 2 A diamond may suffer from fracture during the deposition process due to the high-velocity impact or inter-particle impact between two Cu-Ni-coated diamonds.
- 3 Cold sprayed Al/diamond composites had uniform diamond distribution and high diamond retainability.
- 4 Cold sprayed Al/diamond composites had superior wear-resistance properties that are comparable to selective laser melting Inconel 625 and 17–4PH alloys. Higher diamond contents in the composites resulted in better wear resistance.

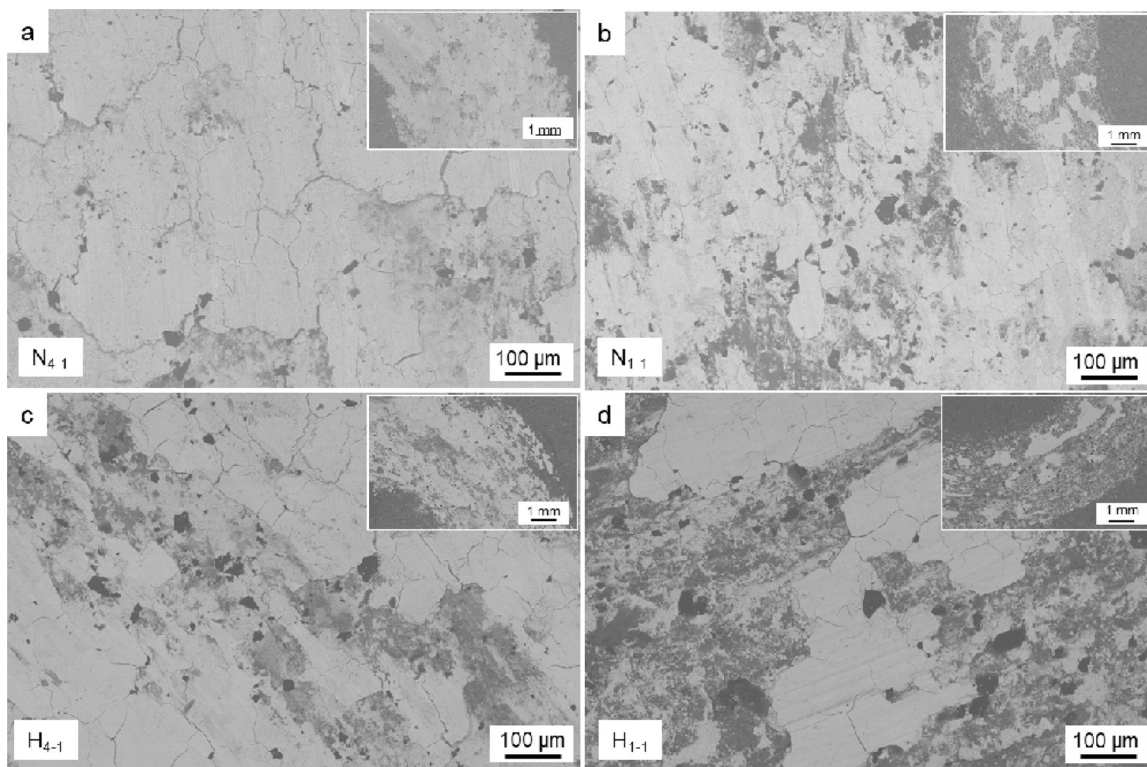


**Fig. 9.** Magnified view of the worn surfaces on the Al/diamond composites under different conditions with the insert image showing the whole worn track.

#### Author statement

About this article, entitled “*Tribological properties of Al/diamond composites produced by cold spray additive manufacturing*”, I would like to declare on behalf of my co-authors that the work described was original research that has not been published previously. Besides, this paper has not under consideration for publication elsewhere, in whole or in part. All the authors of this paper have read and approved the final version submitted.

#### Declaration of Competing Interest

The authors report no conflicts of interest in this work.

#### Acknowledgments

The authors would like to thank the support from the National Natural Science Foundation of China (Grant Nos.51604171, 51690162, 51701112), the Shanghai Science and Technology Committee of China (Grant No. 17JC1400602), Shanghai Sailing Program of China (Grant Nos. 19YF1415900), and Top Research Institution Project of

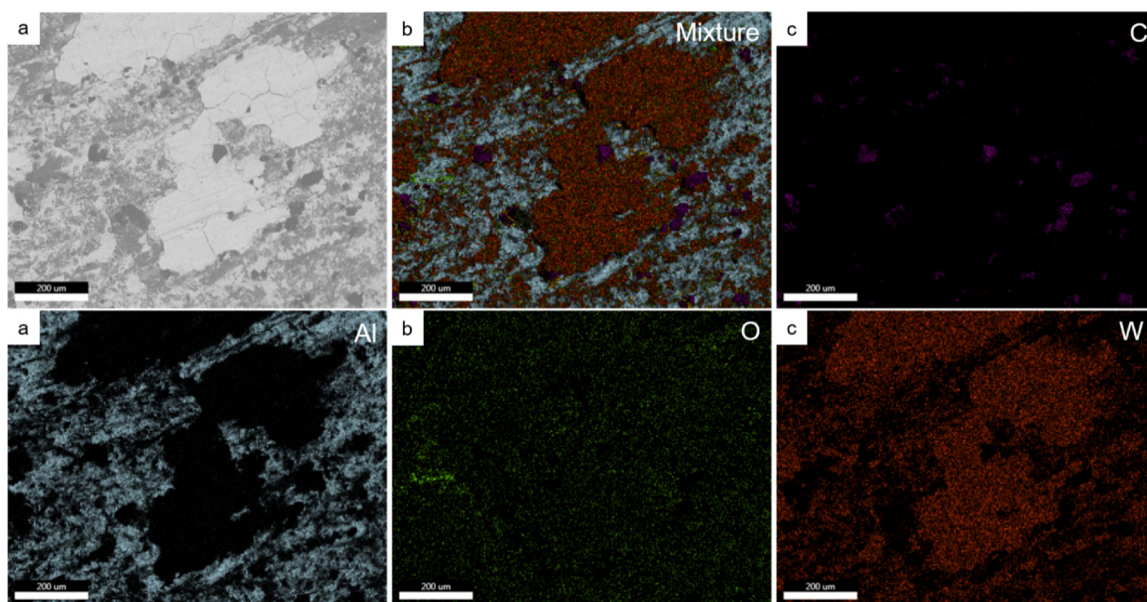


**Fig. 10.** SEM image and EDS mapping on the worn surface of H<sub>1-1</sub> sample after wear test.

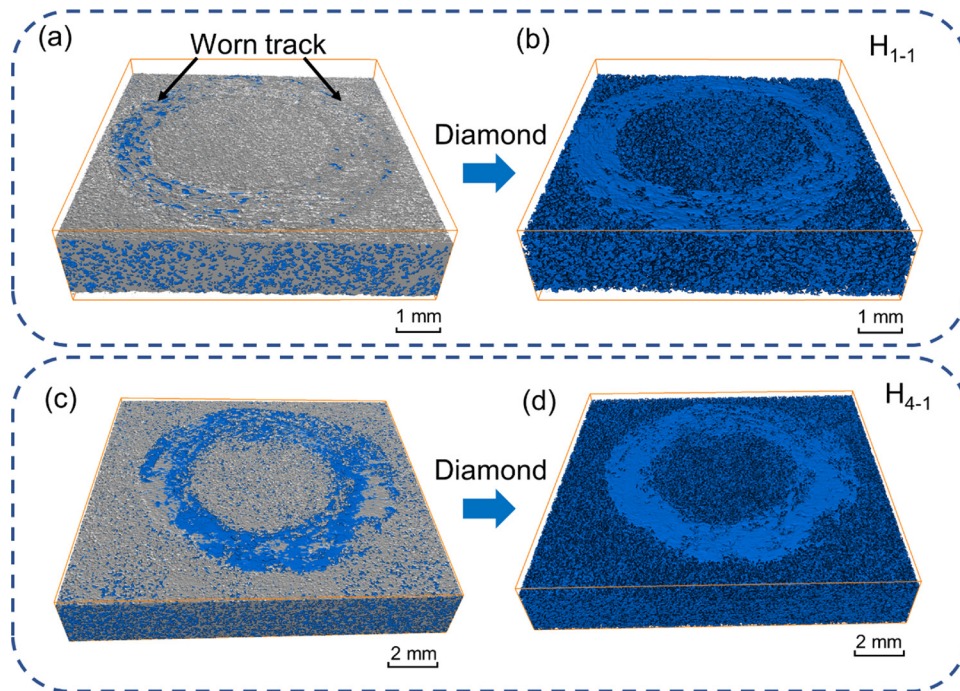


**Fig. 11.** XCT reconstruction of the H1-1 (a-b) and H4-1 (c-d) composites after wear test showing the worn track with gray and blue parts indicating Al and diamond phase respectively: (a) and (c), the diamond/Al composite; (b) and (d) the diamond particles.

Guangdong Academy of Sciences (2020GDASYL-20200302011). The tribological test was assisted by Dr. Liang LAN from Shanghai University of Engineering Science.

## References

- [1] Z. Che, Q. Wang, L. Wang, J. Li, H. Zhang, Y. Zhang, X. Wang, J. Wang, M.J. Kim, Interfacial structure evolution of Ti-coated diamond particle reinforced Al matrix composite produced by gas pressure infiltration, *Composites Part B* 113 (2017) 285–290, <https://doi.org/10.1016/j.compositesb.2017.01.047>.
- [2] I.E. Monje, E. Louis, J.M. Molina, Interfacial nano-engineering in Al/diamond composites for thermal management by in situ diamond surface gas desorption, *Scr. Mater.* 115 (2016) 159–163, <https://doi.org/10.1016/j.scriptamat.2016.01.004>.
- [3] M. Schöbel, H.P. Degenicher, S. Vaucher, M. Hofmann, P. Cloetens, Reinforcement architectures and thermal fatigue in diamond particle-reinforced aluminum, *Acta Mater.* 58 (19) (2010) 6421–6430, <https://doi.org/10.1016/j.actamat.2010.08.004>.
- [4] Z. Tan, G. Ji, A. Addad, Z. Li, J.-F. Silvain, D. Zhang, Tailoring interfacial bonding states of highly thermal performance diamond/Al composites: spark plasma sintering vs. Vacuum hot pressing, *Compos. Part. A* 91 (2016) 9–19, <https://doi.org/10.1016/j.compositesa.2016.09.012>.
- [5] Z. Tan, Z. Li, G. Fan, X. Kai, G. Ji, L. Zhang, D. Zhang, Fabrication of diamond/aluminum composites by vacuum hot pressing: process optimization and thermal properties, *Composites Part B* 47 (2013) 173–180, <https://doi.org/10.1016/j.compositesb.2012.11.014>.
- [6] Z. Tan, Z. Chen, G. Fan, G. Ji, J. Zhang, R. Xu, A. Shan, Z. Li, D. Zhang, Effect of particle size on the thermal and mechanical properties of aluminum composites reinforced with SiC and diamond, *Mater. Des.* 90 (2016) 845–851, <https://doi.org/10.1016/j.matdes.2015.11.028>.
- [7] C. Zhang, Z. Cai, R. Wang, C. Peng, K. Qiu, N. Wang, Microstructure and thermal properties of Al/W-coated diamond composites prepared by powder metallurgy, *Mater. Des.* 95 (2016) 39–47, <https://doi.org/10.1016/j.matdes.2016.01.085>.
- [8] K. Mizuuchi, K. Inoue, Y. Agari, T. Nagaoka, M. Sugioka, M. Tanaka, T. Takeuchi, J.-i. Tani, M. Kawahara, Y. Makino, M. To, Processing of Al/SiC composites in continuous solid-liquid co-existent state by SPS and their thermal properties, *Composites Part B* 43 (4) (2012) 2012–2019, <https://doi.org/10.1016/j.compositesb.2012.02.004>.
- [9] K. Mizuuchi, K. Inoue, Y. Agari, Y. Morisada, M. Sugioka, M. Tanaka, T. Takeuchi, M. Kawahara, Y. Makino, Thermal conductivity of diamond particle dispersed aluminum matrix composites fabricated in solid-liquid co-existent state by SPS, *Composites Part B* 42 (5) (2011) 1029–1034, <https://doi.org/10.1016/j.compositesb.2011.03.028>.
- [10] Y. Zhang, J. Li, L. Zhao, H. Zhang, X. Wang, Effect of metalloid silicon addition on densification, microstructure and thermal-physical properties of Al/diamond composites consolidated by spark plasma sintering, *Mater. Des.* 63 (2014) 838–847, <https://doi.org/10.1016/j.matdes.2014.06.065>.
- [11] W.Z. Shao, V.V. Ivanov, L. Zhen, Y.S. Cui, Y. Wang, A study on graphitization of diamond in copper–diamond composite materials, *Mater. Lett.* 58 (1) (2004) 146–149, [https://doi.org/10.1016/S0167-577X\(03\)00433-6](https://doi.org/10.1016/S0167-577X(03)00433-6).
- [12] J. Yao, L. Yang, B. Li, Z. Li, Beneficial effects of laser irradiation on the deposition process of diamond/Ni60 composite coating with cold spray, *Appl. Surf. Sci.* 330 (2015) 300–308, <https://doi.org/10.1016/j.apsusc.2015.01.029>.
- [13] L. Yang, B. Li, J. Yao, Z. Li, Effects of diamond size on the deposition characteristic and tribological behavior of diamond/Ni60 composite coating prepared by supersonic laser deposition, *Diam. Relat. Mater.* 58 (2015) 139–148, <https://doi.org/10.1016/j.diamond.2015.06.014>.
- [14] A.M. Abyzov, M.J. Kruszewski, Ł. Ciupiński, M. Mazurkiewicz, A. Michalski, K.J. Kurzydłowski, Diamond-tungsten based coating-copper composites with high thermal conductivity produced by Pulse Plasma sintering, *Mater. Des.* 76 (2015) 97–109, <https://doi.org/10.1016/j.matdes.2015.03.056>.
- [15] Z. Tan, Z. Li, G. Fan, X. Kai, G. Ji, L. Zhang, D. Zhang, Diamond/aluminum composites processed by vacuum hot pressing: microstructure characteristics and thermal properties, *Diam. Relat. Mater.* 31 (2013) 1–5, <https://doi.org/10.1016/j.diamond.2012.10.008>.
- [16] Z. Che, Y. Zhang, J. Li, H. Zhang, X. Wang, C. Sun, J. Wang, M.J. Kim, Nucleation and growth mechanisms of interfacial Al4C3 in Al/diamond composites, *J. Alloys. Compd.* 657 (2016) 81–89, <https://doi.org/10.1016/j.jallcom.2015.10.075>.
- [17] T. DebRoy, H.L. Wei, J.S. Zuback, T. Mukherjee, J.W. Elmer, J.O. Milewski, A.M. Beese, A. Wilson-Heid, A. De, W. Zhang, Additive manufacturing of metallic components – process, structure and properties, *Prog. Mater. Sci.* 92 (Supplement C) (2018) 112–224, <https://doi.org/10.1016/j.pmatsci.2017.10.001>.
- [18] E. Hosseini, V.A. Popovich, A review of mechanical properties of additively manufactured Inconel 718, *Addit. Manuf.* 30 (2019) 100877, <https://doi.org/10.1016/j.addma.2019.100877>.
- [19] Y. Ma, G. Ji, X.P. Li, C.Y. Chen, Z.Q. Tan, A. Addad, Z.Q. Li, T.B. Sercombe, J.P. Kruth, On the study of tailorable interface structure in a diamond/Al12Si composite processed by selective laser melting, *Materialia* 5 (2019) 100242, <https://doi.org/10.1016/j.mtla.2019.100242>.
- [20] H. Assadi, H. Kreye, F. Gärtner, T. Klassen, Cold spraying – a materials perspective, *Acta Mater.* 116 (2016) 382–407, <https://doi.org/10.1016/j.actamat.2016.06.034>.
- [21] S. Yin, P. Cavaliere, B. Aldwell, R. Jenkins, H. Liao, W. Li, R. Lupoi, Cold spray additive manufacturing and repair: fundamentals and applications, *Addit. Manuf.* 21 (2018) 628–650, <https://doi.org/10.1016/j.addma.2018.04.017>.
- [22] C. Chen, Y. Xie, X. Yan, S. Yin, R. Huang, R. Zhao, J. Wang, Z. Ren, M. Liu, H. Liao, Effect of hot isostatic pressing (HIP) on microstructure and mechanical properties of Ti6Al4V alloy fabricated by cold spray additive manufacturing, *Addit. Manuf.* (2019), <https://doi.org/10.1016/j.addma.2019.03.028>.
- [23] S. Yin, W. Li, B. Song, X. Yan, M. Kuang, Y. Xu, K. Wen, R. Lupoi, Deposition of FeCoNiCrMn high entropy alloy (HEA) coating via cold spraying, *J. Mater. Sci. Technol.* 35 (6) (2019) 1003–1007, <https://doi.org/10.1016/j.jmst.2018.12.015>.
- [24] S. Yin, Y. Xie, J. Cizek, E.J. Ekoi, T. Hussain, D.P. Dowling, R. Lupoi, Advanced diamond-reinforced metal matrix composites via cold spray: properties and deposition mechanism, *Composites Part B* 113 (2017) 44–54, <https://doi.org/10.1016/j.compositesb.2017.01.009>.
- [25] C. Chen, X. Xie, Y. Xie, M.-P. Planche, S. Deng, G. Ji, E. Aubry, Z. Ren, H. Liao, Cold spraying of thermally softened Ni-coated FeSiAl composite powder: microstructure

- characterization, tribological performance and magnetic property, *Mater. Des.* 160 (2018) 270–283, <https://doi.org/10.1016/j.matdes.2018.09.025>.
- [26] L.-S. Wang, H.-F. Zhou, K.-J. Zhang, Y.-Y. Wang, C.-X. Li, X.-T. Luo, G.-J. Yang, C.-J. Li, Effect of the powder particle structure and substrate hardness during vacuum cold spraying of Al<sub>2</sub>O<sub>3</sub>, *Ceram. Int.* 43 (5) (2017) 4390–4398, <https://doi.org/10.1016/j.ceramint.2016.12.085>.
- [27] C. Lee, J. Kim, Microstructure of kinetic spray coatings: a review, *J. Therm. Spray. Technol.* 24 (4) (2015) 592–610, <https://doi.org/10.1007/s11666-015-0223-5>.
- [28] X.-T. Luo, C.-X. Li, F.-L. Shang, G.-J. Yang, Y.-Y. Wang, C.-J. Li, High velocity impact induced microstructure evolution during deposition of cold spray coatings: a review, *Surf. Coat. Technol.* 254 (2014) 11–20, <https://doi.org/10.1016/j.surfcoat.2014.06.006>.
- [29] M.R. Rokni, S.R. Nutt, C.A. Widener, V.K. Champagne, R.H. Hrabe, Review of relationship between particle deformation, coating microstructure, and properties in high-pressure cold spray, *J. Therm. Spray. Technol.* 26 (6) (2017) 1308–1355, <https://doi.org/10.1007/s11666-017-0575-0>.
- [30] A. Vilardell, N. Cinca, A. Concastell, S. Dosta, I. Cano, J. Guilemany, Cold spray as an emerging technology for biocompatible and antibacterial coatings: state of art, *J. Mater. Sci.* 50 (13) (2015) 4441–4462.
- [31] W. Li, K. Yang, S. Yin, X. Yang, Y. Xu, R. Lupoi, Solid-state additive manufacturing and repairing by cold spraying: a review, *J. Mater. Sci. Technol.* 34 (3) (2017) 440–457, <https://doi.org/10.1016/j.jmst.2017.09.015>.
- [32] C. Chen, S. Gojon, Y. Xie, S. Yin, C. Verdy, Z. Ren, H. Liao, S. Deng, A novel spiral trajectory for damage component recovery with cold spray, *Surf. Coat. Technol.* 309 (2017) 719–728, <https://doi.org/10.1016/j.surfcoat.2016.10.096>.
- [33] D. Herzog, V. Seyda, E. Wycisk, C. Emmelmann, Additive manufacturing of metals, *Acta Mater.* 117 (2016) 371–392, <https://doi.org/10.1016/j.actamat.2016.07.019>.
- [34] R.N. Raoelison, Y. Xie, T. Sapanathan, M.P. Planche, R. Kromer, S. Costil, C. Langlade, Cold gas dynamic spray technology: a comprehensive review of processing conditions for various technological developments till to date, *Addit Manuf* 19 (2018) 134–159, <https://doi.org/10.1016/j.addma.2017.07.001>.
- [35] K. Spencer, D.M. Fabijanic, M.X. Zhang, The use of Al-Al<sub>2</sub>O<sub>3</sub> cold spray coatings to improve the surface properties of magnesium alloys, *Surf. Coat. Technol.* 204 (3) (2009) 336–344, <https://doi.org/10.1016/j.surfcoat.2009.07.032>.
- [36] S. Kumar, S.K. Reddy, S.V. Joshi, Microstructure and performance of cold sprayed Al-SiC composite coating with high fraction of particulates, *Surf. Coat. Technol.* 318 (2017) 62–71, <https://doi.org/10.1016/j.surfcoat.2016.11.047>.
- [37] M. Yu, X.K. Suo, W.Y. Li, Y.Y. Wang, H.L. Liao, Microstructure, mechanical property and wear performance of cold sprayed Al5056/SiCp composite coatings: effect of reinforcement content, *Appl. Surf. Sci.* 289 (2014) 188–196, <https://doi.org/10.1016/j.apsusc.2013.10.132>.
- [38] T. Peat, A. Galloway, A. Toumpis, P. McNutt, N. Iqbal, The erosion performance of particle reinforced metal matrix composite coatings produced by co-deposition cold gas dynamic spraying, *Appl. Surf. Sci.* 396 (2017) 1623–1634, <https://doi.org/10.1016/j.apsusc.2016.10.155>.
- [39] W.-Y. Li, C. Yang, H. Liao, Effect of vacuum heat treatment on microstructure and microhardness of cold-sprayed TiN particle-reinforced Al alloy-based composites, *Mater. Des.* 32 (1) (2011) 388–394, <https://doi.org/10.1016/j.matdes.2010.06.002>.
- [40] W.Y. Li, G. Zhang, H.L. Liao, C. Coddet, Characterizations of cold sprayed TiN particle reinforced Al2319 composite coating, *J. Mater. Process. Technol.* 202 (1) (2008) 508–513, <https://doi.org/10.1016/j.jmatprotec.2007.09.045>.
- [41] P. Cavaliere, A. Perrone, A. Silvello, Mechanical and microstructural behavior of nanocomposites produced via cold spray, *Composites Part B* 67 (2014) 326–331, <https://doi.org/10.1016/j.compositesb.2014.07.023>.
- [42] X.-T. Luo, C.-J. Li, Large sized cubic BN reinforced nanocomposite with improved abrasive wear resistance deposited by cold spray, *Mater. Des.* 83 (2015) 249–256, <https://doi.org/10.1016/j.matdes.2015.06.009>.
- [43] O. Meydanoglu, B. Jodoin, E.S. Kayali, Microstructure, mechanical properties and corrosion performance of 7075 Al matrix ceramic particle reinforced composite coatings produced by the cold gas dynamic spraying process, *Surf. Coat. Technol.* 235 (2013) 108–116, <https://doi.org/10.1016/j.surfcoat.2013.07.020>.
- [44] D.J. Woo, F.C. Heer, L.N. Brewer, J.P. Hooper, S. Osswald, Synthesis of nanodiamond-reinforced aluminum metal matrix composites using cold-spray deposition, *Carbon* 86 (2015) 15–25, <https://doi.org/10.1016/j.carbon.2015.01.010>.
- [45] P. Das, S. Paul, P.P. Bandyopadhyay, Preparation of diamond reinforced metal powders as thermal spray feedstock using ball milling, *Surf. Coat. Technol.* 286 (2016) 165–171, <https://doi.org/10.1016/j.surfcoat.2015.12.022>.
- [46] S. Yin, J. Cizek, C. Chen, R. Jenkins, G. O'Donnell, R. Lupoi, Metallurgical bonding between metal matrix and core-shelled reinforcements in cold sprayed composite coating, *Scr. Mater.* 177 (2020) 49–53, <https://doi.org/10.1016/j.scriptamat.2019.09.023>.
- [47] S. Dosta, M. Couto, J.M. Guilemany, Cold spray deposition of a WC-25Co cermet onto Al7075-T6 and carbon steel substrates, *Acta Mater.* 61 (2) (2013) 643–652, <https://doi.org/10.1016/j.actamat.2012.10.011>.
- [48] S. Yin, M. Meyer, W. Li, H. Liao, R. Lupoi, Gas Flow, Particle acceleration, and heat transfer in cold spray: a review, *J. Therm. Spray. Technol.* 25 (5) (2016) 874–896, <https://doi.org/10.1007/s11666-016-0406-8>.
- [49] S. Yin, X.K. Suo, Y.C. Xie, W.Y. Li, R. Lupoi, H.L. Liao, Effect of substrate temperature on interfacial bonding for cold spray of Ni onto Cu, *J. Mater. Sci.* 50 (22) (2015) 7448–7457, <https://doi.org/10.1007/s10853-015-9304-6>.
- [50] S. Guetta, M.H. Berger, F. Borit, V. Guiptom, M. Jeandin, M. Boustie, Y. Ichikawa, K. Sakaguchi, K. Ogawa, Influence of particle velocity on adhesion of cold-sprayed splats, *J. Therm. Spray. Technol.* 18 (3) (2009) 331–342, <https://doi.org/10.1007/s11666-009-9327-0>.
- [51] H. Na, G. Bae, S. Shin, S. Kumar, H. Kim, C. Lee, Advanced deposition characteristics of kinetic sprayed bronze/diamond composite by tailoring feedstock properties, *Compos. Sci. Technol.* 69 (3) (2009) 463–468, <https://doi.org/10.1016/j.compscitech.2008.11.015>.
- [52] L.-Y. Chen, H. Konishi, A. Fehrenbacher, C. Ma, J.-Q. Xu, H. Choi, H.-F. Xu, F.E. Pfefferkorn, X.-C. Li, Novel nanoprocessing route for bulk graphene nanoplatelets reinforced metal matrix nanocomposites, *Scr. Mater.* 67 (1) (2012) 29–32, <https://doi.org/10.1016/j.scriptamat.2012.03.013>.
- [53] G. Iacob, V.G. Ghica, M. Buzatu, T. Buzatu, M.I. Petrescu, Studies on wear rate and micro-hardness of the Al/Al<sub>2</sub>O<sub>3</sub>/Gr hybrid composites produced via powder metallurgy, *Composites Part B* 69 (2015) 603–611, <https://doi.org/10.1016/j.compositesb.2014.07.008>.
- [54] N. Yang, J. Boselli, I. Sinclair, Simulation and quantitative assessment of homogeneous and inhomogeneous particle distributions in particulate metal matrix composites, *J. Microsc.* 201 (2) (2001) 189–200, <https://doi.org/10.1046/j.1365-2818.2001.00766.x>.
- [55] K.J. Hodder, H. Izadi, A.G. McDonald, A.P. Gerlich, Fabrication of aluminum-alumina metal matrix composites via cold gas dynamic spraying at low pressure followed by friction stir processing, *Mater. Sci. Eng. A* 556 (2012) 114–121, <https://doi.org/10.1016/j.msea.2012.06.066>.
- [56] E. Irissou, J.-G. Legoux, B. Arsenault, C. Moreau, Investigation of Al-Al<sub>2</sub>O<sub>3</sub> cold spray coating formation and properties, *J. Therm. Spray. Technol.* 16 (5) (2007) 661–668, <https://doi.org/10.1007/s11666-007-9086-8>.
- [57] D.J. Woo, B. Sneed, F. Peerally, F.C. Heer, L.N. Brewer, J.P. Hooper, S. Osswald, Synthesis of nanodiamond-reinforced aluminum metal composite powders and coatings using high-energy ball milling and cold spray, *Carbon* 63 (2013) 404–415, <https://doi.org/10.1016/j.carbon.2013.07.001>.
- [58] R. Jenkins, S. Yin, B. Aldwell, M. Meyer, R. Lupoi, New insights into the in-process densification mechanism of cold spray Al coatings: low deposition efficiency induced densification, *J. Mater. Sci. Technol.* 35 (3) (2019) 427–431, <https://doi.org/10.1016/j.jmst.2018.09.045>.
- [59] Y. Xie, C. Chen, M.-P. Planche, S. Deng, R. Huang, Z. Ren, H. Liao, Strengthened peening effect on metallurgical bonding formation in cold spray additive manufacturing, *J. Therm. Spray. Technol.* 28 (4) (2019) 769–779, <https://doi.org/10.1007/s11666-019-00854-4>.